NO_2 Chemiluminescent Wake Radiation

RICHARD L. SCHAPKER* AND MORTON CAMAC*
Avco Everett Research Laboratory, Everett, Mass.

A flowfield and chemical kinetics model is presented for calculating the $NO + O \rightarrow NO_2 + h\nu$ chemiluminescence wake emission. Numerical results are compared to the wake measurements made by Reis in a ballistic range. The wake NO_2 chemiluminescence intensity tends to peak at several hundred body diameters, decreasing in intensity in the far wake. The far-wake structure of these profiles is fit well by our calculations. Peaking of the intensity is mainly because of the drop in the mean wake temperature; final decay is shown to be caused both by atomic O cleanup and by dilution in the growing turbulent wake. For pure air, the cleanup reactions are due to $NO + O + N_2 \rightarrow NO_2 + N_2$ and $O_2 + O + N_2 \rightarrow O_3 + N_2$. However, for the ballistic range conditions with approximately 0.01% H_2O contamination, our calculations indicate that O cleanup can be affected to a measurable degree by a reaction chain involving atomic hydrogen.

I. Introduction

THE strong bow shock in front of blunt hypervelocity vehicles produces considerable oxygen dissociation. The atomic oxygen is convected around the body, and a substantial quantity survives to the far wake, thus becoming an important source of chemical (latent) energy even after the wake has cooled to ambient conditions. For a sphere at velocities of 23,000 fps, more than one-third of the incident flow energy resides in the oxygen dissociation. Chemiluminescent and chemidetachment reactions involving the recombination of atomic oxygen can produce considerable amounts of radiation; several sources of pure air chemiluminescent emission are the recombination radiation from N_2 (1st positive, Lewis-Rayleigh yellow afterflow), O_2 (Schumann-Runge), NO (β and γ bands), and NO_2 continuum.

Reis[1] has measured wake radiation emission from nonablating spheres at flight velocities from 14 to 21 kft/sec. He demonstrated that the visible and near *IR* wake emission for nonablating spheres is due to the NO_2 continuum. The spectral distribution of far wake radiation was consistent with the $NO + O \rightarrow NO_2 + h\nu$ spectrum,[2] and using a relatively simple model he showed that the intensities were consistent with those to be expected from NO_2 chemiluminescence.[2]

In addition, the near wake ultraviolet data[1] are consistent with O_2 Schumann-Runge chemiluminescence. The use of this O_2 radiation for studying near wake turbulent mixing and obtaining wake temperature fluctuations is treated in another paper.[3]

In this paper, we compare intensity measurements with theoretical calculations for NO_2 emission. Our flowfield computations are divided into two regions: 1) the flow downstream of the bow shock, around the body (neglecting boundary-layer effects) and in the near wake is obtained from an inviscid stream-line calculation including nonequilibrium chemistry. This specifies the species concentrations and temperature of the flow into the far wake. 2) NO_2 wake radiation is calculated using a one-dimensional procedure. The gas entrained by the growing turbulent wake is assumed to mix immediately and homogeneously; thus, the turbulent portion of the wake has uniform temperature and species across the wake. This approximation is valid because 1) this radiation intensity has a relatively weak temperature dependence and 2) the chemical reaction times are much slower than the turbulent mixing times.

Presented as Paper 68-702 at the AIAA Fluid and Plasma Dynamics Conference, Los Angeles, Calif., June 24–26, 1968; submitted July 19, 1968; revision received June 23, 1969. This research was supported by the Advanced Research Projects Agency of the Department of Defense and Space and Missile Systems Organization, Air Force Systems Command and was monitored by Space and Missile Systems Organization, Air Force Systems Command under Contract F04701-68-C-0036. The authors are indebted to R. Yanover of Avco Everett Research Laboratory for his efforts relating to the programing and execution of the flowfield and wake computation programs and to J. Ryan for typing the text.

* Principal Research Scientists.

II. Calculation Procedure

In this section, we discuss the aerodynamic and chemical models for calculating NO_2 wake chemiluminescence. Specific wake radiation calculations are presented in Sec. IV, where they are compared to the ballistic range data of Reis.[1]

Our computation of hypersonic blunt-body flowfield properties is performed in three steps. 1) The nonequilibrium fluid properties around the body and near wake are determined according to the laminar stream-tube approach of Lin and Teare.[4] Boundary-layer effects were neglected. 2) A turbulent wake is superimposed onto the flow pattern of step 1 by specifying an average turbulent wake boundary obtained from experimental measurements. This determines the entrainment history of chemical species and thermal energy along the turbulent wake front. 3) Average turbulent wake properties are computed from the input supplied by steps 1 and 2 using the procedure of Sutton.[5] With this over-all procedure in mind, we will now discuss important features of each step.

Inviscid Flowfield

The chemically reacting, laminar, inviscid flowfield of a sphere in hypersonic flight is computed by the stream-tube method of Lin and Teare.[4] This approach is based on forward integration of the chemical rate equations, without diffusion, along stream lines from a point immediately downstream of the bow shock. Total enthalpy is constant along all stream lines, and is equal to the freestream value. Velocities along stream lines are determined by integration of the inviscid momentum equation $dp + VdV = 0$ in conjunction with a specified pressure distribution. The pressure

history used in the present calculations follows closely that given by Lin and Hayes.[6]

The shock shapes used for all our calculations are obtained from a correlation of sphere bow-shock measurements by Korkan.[7] His correlation is a function of freestream Mach number M_∞ and the equilibrium density ratio across a normal shock at the freestream pressure and M_∞. Nonequilibrium calculations for the cases considered herein show that approximate chemical equilibrium is achieved on the stagnation stream line between the shock and stagnation point, thus justifying use of the equilibrium normal shock density ratio in the shock-shape correlation.

Generally, sixteen streamlines are computed for each flowfield, spaced at distances from the flight axis upstream of the shock between 0 and 1.5 R_N, where R_N is the nose radius. Stream lines entering the shock at larger radii undergo negligible chemistry, so that the temperature along these is given directly by the isentropic pressure-temperature relation with $\gamma = 1.4$.

Inviscid Flow Chemistry

Chemical relaxation along stream lines in the decreasing pressure environment of the inviscid flowfield is determined by specifying appropriate reactions and reaction rates. Because of the large computing times involved in computing inviscid concentration histories, a chemical model including only the major species O_2, N_2, NO, O, and N is used for the inviscid flow.

Reactions used for the inviscid flow are given in Ref. 8. Calculations have shown that omission of the triatomic and polyatomic species has a minor effect on inviscid concentrations and temperatures for blunt bodies. In the lower-temperature regions of the wake triatomic reactions must be included, but here, too, simplifications in the chemical model result from the nature of the wake environment. (These are discussed in Sec. III.)

Typical results of inviscid flow calculations, from one of the ballistic range cases considered, are shown in Figs. 1 and 2. The species mole ratios and temperature change relatively slowly along stream lines as one progresses downstream. Since the stream-line radii are also varying slowly (e.g., at $x/R_N = 400$, they are only $\sim$10% greater than at $x/R_N = 100$) the profiles as shown give a good approximation to the reacting flow environment into which the turbulent wake grows.

Wake Growth: Front Values

The entrainment history of active species and thermal energy is determined by the rate at which the turbulent

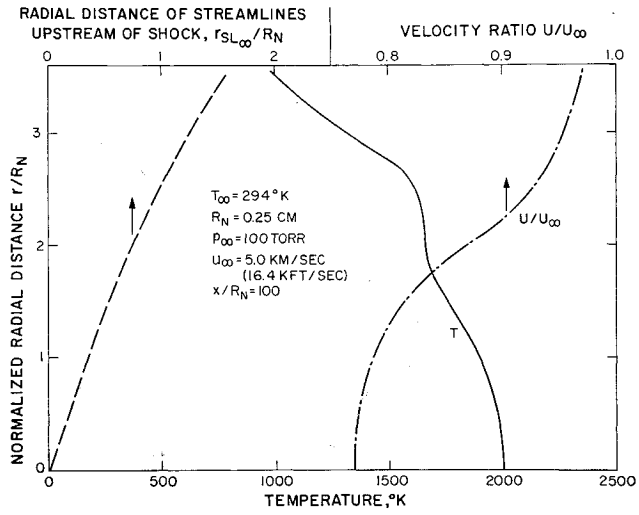

Fig. 2 Radial variation of temperature and velocity ratio for the same inviscid flowfield calculation as Fig. 1.

wake edge grows outward along the inviscid profiles. Thus, wake growth is the principal link between the reacting inviscid field and the wake flow.

For the sphere shots considered herein, Reynolds numbers $U_\infty R_N/\nu_\infty = Re_\infty$ were above 0.8 (10^5). Transition data[9] indicate that sphere wakes become turbulent within the first 20 nose radii for $Re_\infty \gtrsim 0.5(10^5)$. Thus, for present purposes, the wakes are assumed to be turbulent from the neck on.

Axisymmetric turbulent wake width measurements[10-12] exhibit a $\frac{1}{3}$ power growth at a distance of about $x/R_N \sim 200$ for $Re_\infty \gtrsim 0.5(10^5)$. In this analysis, we are interested in the NO_2 radiation in the vicinity, and downstream, of the peak, which occurs at $x/R_N \sim 800$. Hence a pure $\frac{1}{3}$ growth law was used for the calculations, given by

$$R_f/R_N = 0.7(x/R_N)^{1/3} \tag{1}$$

Using this wake-growth relation, entrainment histories of species and temperature were calculated, typical examples of which are shown in Fig. 3. It can be mentioned that divergence from the $\frac{1}{3}$ growth in the near wake changes markedly the entrainment histories close to the body.[8] However, under the present ballistic range conditions, the chemistry proceeds sufficiently slowly that such differences in near-wake entrainment histories have a negligible effect on the concentrations and temperature in the wake at $x/R_N \sim 200$.

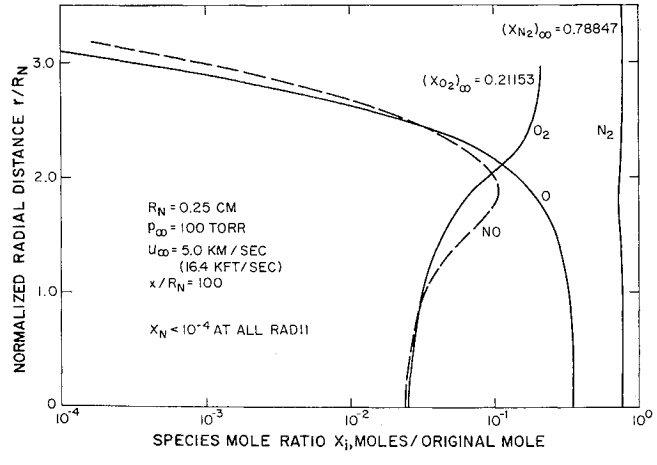

Fig. 1 Radial variation of species mole ratios in the inviscid flowfield corresponding to a pure-air nonequilibrium stream-tube calculation for the conditions indicated.

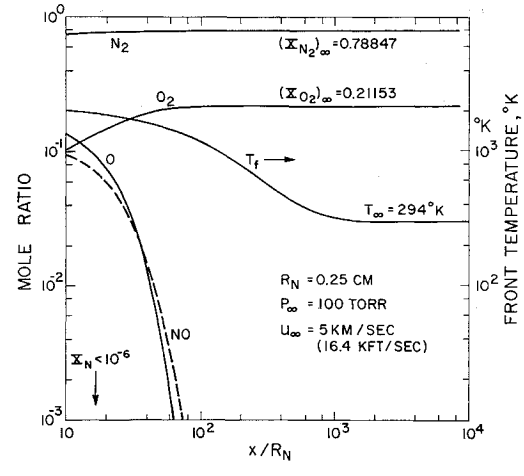

Fig. 3 Flow properties along average turbulence front obtained from inviscid flowfield calculations and pure $\frac{1}{3}$ wake growth.

Wake Calculation Scheme

The wake calculation procedure which one adopts depends on the nature of the observable(s) under consideration. The dependence of NO_2 chemiluminescence on its governing variables is such that a simple, one-dimensional description of wake properties is sufficient.[8]

Accordingly, our predictions of NO_2 wake intensity are obtained from a one-dimensional procedure described by Sutton,[5] modified for variable C_p of the front gas. This wake flow model is based on the assumption of instantaneous, homogeneous mixing of ingested fluid properties, as originally proposed by Lin and Hayes.[6]

The calculation is started at $x/R_N = 200$. From Fig. 3, this is beyond the entrainment cutoff of O and NO, so that only O_2 and N_2 are ingested at the local front temperature. Input items to the wake program are thus initial (average) temperature and species concentrations, and front temperatures determined from the inviscid flow calculation as described previously.

It should be emphasized at this point that the calculational procedures just described comprise essentially one single computation system which is executed from start to finish with no adjustment in any parameters. Aside from the chemistry, the variables in the program are 1) the shock shape, 2) inviscid stream-line pressure distributions, and 3) the wake front values. These have been built into the program using what we consider the best theoretical or experimental information, and are determined in a consistent manner from case to case.

Equation for NO_2 Radiation

We complete the calculation scheme description with the relation for wake NO_2 emission. NO_2 chemiluminescence arises from radiative transitions from the recombination of O and NO to form NO_2

$$NO + O \xrightarrow{k_1} NO_2 + h\nu \tag{2}$$

where k_1 is the observed rate constant for the total radiation, with a value,[2,13,14]

$$k_1 = 6.5(10^{-12})T^{-2} \text{ cm}^3\text{sec}^{-1}$$

The photons emitted have a broad continuum spectrum from 0.4μ to over 1μ.

For wake conditions of interest herein, the gas is optically thin and self-absorption effects are negligible. The energy radiated per steradian per unit volume of wake gas is

$$d^3I_{NO2}/rdrd\theta dx = h\bar{\nu}k_1[O][NO]/4\pi \tag{3}$$

where [ ] denotes number density of the indicated species, and $rdrd\theta dx$ is the volume element. $h\bar{\nu}$ is the photon energy averaged over the observed spectrum. Equation (3), integrated over a wake volume Δx units long, is given by[8]

$$I_{NO2}(x)/\Delta x = (h\bar{\nu}/4)k_1(T_{av})[O]_{av}[NO]_{av}R_f^2 \tag{4}$$

where subscript "av" denotes one-dimensional wake values. This expression is based on approximations which probably restrict its validity to the far wake, i.e., to distances greater than $x/R_N \sim 200$.

III. NO_2 Intensity Scaling and Wake Chemistry

We will now discuss scaling of NO_2 wake emission and relevant chemical kinetic aspects of wake flow. In particular, the previous section brought out the dependence of NO_2 intensity on the concentration of O and NO in the wake as well as the average temperature. Hence, NO_2 scaling will depend on 1) the flux of chemically active species O and NO into the wake, 2) temperature along stream lines at the wake boundary, i.e., front temperature history, and 3) chemical reactions in the turbulent wake which deplete the O and NO.

Scaling Considerations

To develop scaling relations, we will write the NO_2 intensity relation, Eq. (4), in terms of factors which show explicitly its dependence on ambient pressure, body size, and bow-shock and wake chemistry. In order to separate out more clearly effects due to chemistry, it is convenient to ratio average number densities $[O]_{av}$ and $[NO]_{av}$ to the values in the absence of wake chemistry $[O]'_{av}$ and $[NO]'_{av}$. These ratios are denoted by $\psi(x)$,

$$\psi_O(x) = [O]_{av}/[O]'_{av}, \ \psi_{NO}(x) = [NO]_{av}/[NO]'_{av} \tag{5}$$

In the absence of chemical production of a species, the average number density decreases only by dilution. Thus,

$$R_f^2[NO]'_{av} = \text{const} = \{R_f^2[NO]'_{av}\}_{x_0} \tag{6}$$

where similarly for $[O]'_{av} \cdot x_0$ is the initial axial position.

It was seen in Fig. 3 that O and NO are deposited into the wake within the first 100 nose radii or so. Over this entrainment distance, the O and NO react sufficiently slowly that no significant change takes place in the total number O and NO particles. Thus, the total flux of O and NO particles initially deposited into the wake is given by integration over the inviscid streamlines at the station $x = x_0$. We define dimensionless flux parameters χ as

$$\chi_O = (R_N^2U_\infty N_\infty)^{-1}\left(\int_0^\infty U[O]2rdr\right)_{x_0} \tag{7}$$

and similarly for χ_{NO}, where

$$N_\infty = p_\infty/kT_\infty \tag{8}$$

The denominator in Eq. (7) represents the ambient particle flux intercepted by the body. In terms of the one-dimensional wake fluxes, one thus has

$$\left(\int_0^\infty U[O]2rdr\right)_{x_0} = (R_f^2U_{av}[O]'_{av})_{x_0}$$

Combining this with Eqs. (5–7) yields

$$[O]_{av} = N_\infty\chi_O\psi_O/Y_f^2 \text{ and } [NO]_{av} = N_\infty\chi_{NO}\psi_{NO}/Y_f^2 \tag{9}$$

where $Y_f = R_f/R_N$ and we have set $(U_{av})_{x_0} = U_\infty$.

Therefore, with $k_1 = k_0T^{-2}$, Eq. (4) becomes

$$I_{NO2}(x)/\Delta x = (h\bar{\nu}k_0/4)(N_\infty R_N)^2\chi_O\chi_{NO}[\psi_O\psi_{NO}(Y_fT_{av})^{-2}] \tag{10}$$

The bracketed factors depend upon the chemical kinetics, growth, and average temperature of the turbulent wake, and are discussed in the following part: "Turbulent Wake Scaling." On the other hand, χ_O and χ_{NO} depend upon the inviscid chemistry between the bow shock and the O-, NO-entrainment cutoff. The product $N_\infty R_N$, or its equivalent, $p_\infty d$, is the explicit dependence upon ambient pressure and body size.

Turbulent Wake Scaling

The simplest type of scaling is $p_\infty d$ scaling, usually referred to as binary scaling. For the variation of inviscid species-flux parameters χ_O and χ_{NO} with $p_\infty d$, a number of flowfield calculations were performed with results shown in Figs. 4 and 5. Strictly speaking, binary scaling would require these inviscid flux parameters to be constant at a given velocity. It is seen that this is true only to a rough approximation, especially for the small bodies, since both parameters vary by a factor somewhat greater than 2 over the calculated ranges. Thus, all other things being equal, scaling within the range of $p_\infty d$ from 0.01 to 0.1 could produce uncertainty within a factor of about 2 in the intensity.

Consideration will now be given to the bracketed factors in Eq. (10) which depend on turbulent wake chemistry, temperature, and growth. Three important cases will be treated: A) no wake chemistry, B) wake chemistry when there is negligible atomic nitrogen, and C) wake chemistry at high velocities with appreciable amounts of atomic N. It will be shown that in case B only the O recombination is important. In case C the wake chemistry is more involved and depends to a large extent on details of turbulent mixing rates in the near wake.

Case A. No Wake Chemistry

When there is no net chemical production of O and NO in the wake, $\psi_O = \psi_{NO} = 1$ at all x. Then Eq. (10) reduces to

$$I_{NO_2}(x)/\Delta x = (h\bar{\nu}/4)k_0(N_\infty R_N)^2\chi_O\chi_{NO}Y_f^{-2}T_{av}^{-2} \quad (11)$$

This expression gives the essential features of NO_2 wake emission in the limit of low ambient pressures. Thus, Eq. (11) provides insight into the scaling of the observed NO_2 intensity peak.

Initially, the wake temperature is high, which tends to reduce the NO_2 intensity. Proceeding downstream, the temperature drops as Y_f (with corresponding dilution) increases, and it is the opposing effect of each which produces the NO_2 intensity peak. At low pressures, there is no chemistry, and the temperature T_{av} drops faster then Y_f^2 from ingestion of the rapidly decreasing thermal energy along the front (see Fig. 3) in the region $x/R_N \sim 200$ to 800. This fast decrease in T_{av} drives the NO_2 intensity up, until the point is reached where T_{av} begins to decrease less rapidly. Thus, the intensity peaks, and beyond this point dilution of O and NO takes over; in the far wake where $T_{av} \approx T_\infty$, dilution of O and NO controls the NO_2 intensity decay in the absence of chemistry.

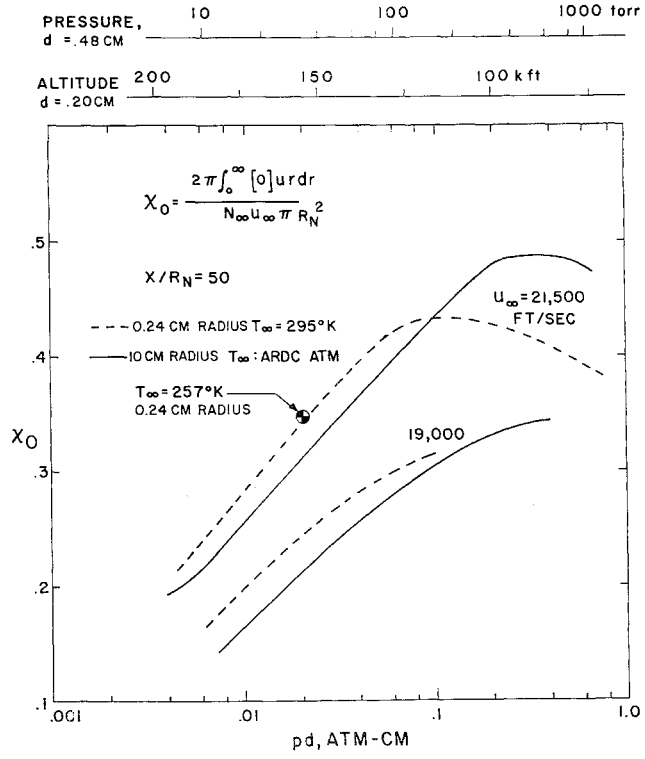

Fig. 4 Inviscid flux parameter for atomic oxygen at 50 body radii normalized by the flux of ambient particles within the sphere frontal area. It has been found for the two spheres by inviscid flowfield calculations. The ambient temperature for the small sphere has been taken to be 295°K whereas, for the large sphere, it was taken from the ARDC 1962 Standard Atmosphere. One calculation, indicated by ⊖, has been made using the scaled temperature 257°K for the small sphere to show the insensitivity of the results of the inviscid flowfield calculation to the choice of ambient temperature.

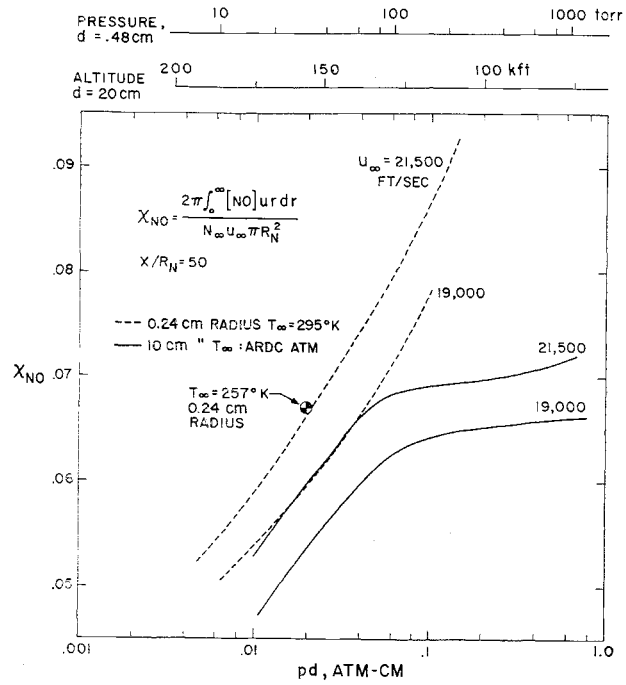

Fig. 5 The inviscid flux parameter for nitric oxide.

We have already discussed scaling of χ_O and χ_{NO}. The dimensionless wake radius Y_f scales with $p_\infty d$. It remains to investigate scaling of the average temperature.

The average wake temperature can be regarded as a measure of the thermal energy flux across a wake cross section, and is $(C_pTU)_{av}\pi R_f^2$. However, sufficiently far downstream, $C_p \approx C_{p\infty}$ and $U \approx U_\infty$; since R_f exhibits binary scaling, we can consider T_{av} alone as representing the thermal energy ingested from the inviscid flowfield, and thus look at its variation with $p_\infty d$ at a given U_∞ and x.

In Fig. 6 are presented results from a series of wake calculations which cover the range of body sizes from 0.24 to 10 cm for the indicated velocities. The axial stations $x/R_N = 400$ and 1000 were selected as being representative of 1) the relatively hot wake but not far enough for appreciable chemistry to take place and 2) the cooler wake regions after all

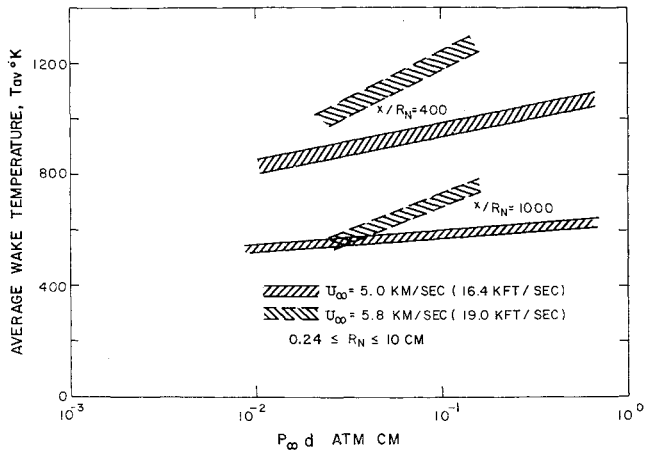

Fig. 6 Average wake temperature at two axial stations as a function of the binary scale parameter. Values shown are results of a one-dimensional calculation based on instantaneous mixing of fluid ingested through the wake front.

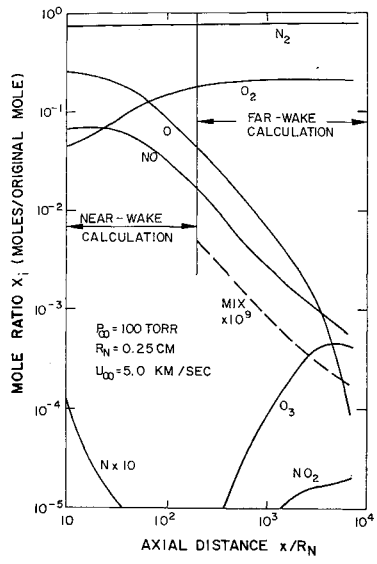

Fig. 7 Results of one-dimensional wake calculations of species mole ratios. The dashed line corresponds to a chemically inert trace species which undergoes pure dilution in the wake.

of the inviscid flowfield thermal energy has been ingested. Higher velocities are seen to have a larger effect on average temperatures with increasing $p_\infty d$. However, the variation in T_{av} over the range of $p_\infty d$ shown at a given velocity amounts to less than a factor of 2 in the temperature dependence of NO_2 intensity. Thus, $p_\infty d$ scaling of wake temperature holds fairly well; even with O and NO chemistry, the effect on wake temperature is small.

Case B. Wake Chemistry with Negligible Atomic N

The important wake chemical reactions are given in Table 1. Depletion of NO in the wake involves primarily reactions with N, so that for $U_\infty < 20{,}000$ fps the amount of NO in the wake remains constant, i.e., $\psi_{NO} = 1$ at all x.[8] Atomic O removal takes place chiefly at a rate given by,[8]

$$(dln[O]/dt)_{chem} \approx -2[M]\{k_4[NO] + k_3[O_2] + k_{18}[O]\} \quad (12)$$

where $[M]$ denotes gas number density.

Equation (12) has no adjustable parameters, since the rate constants k_4, k_3, and k_{18} are known fairly accurately.[8] The three reactions in this relation are important in different regions of the flow. Reaction 18 dominates in the inviscid flow around the body and near wake. Within the turbulent wake both reactions 4 and 3 are important for the first few thousands of body diameters, after which reaction 3 dominates.

When the atomic N concentration is negligible, NO chemistry does not change the number of NO molecules until very far downstream ($x/R_N > 8000$). Reaction 4 is the principle depletion path for NO, but reaction 6 restores NO at almost the same rate during the first few thousand body diameters, resulting in a negligible net chemical production of NO.

The three reactions in Eq. (12) are important for the O-recombination and each requires three-body collisions. In the cooler regions of the wake $[M] \approx [M]_\infty$ and $[O]_2 \approx [M]_\infty/5$. It follows from Eq. (12) that far-wake NO_2 intensity decay scaling is

$$-dln[O]/d(x/d) \propto p_\infty{}^2 d$$

Thus, experiments with small bodies in ballistic ranges give NO_2 chemiluminescent wakes shorter than predicted from simple $p_\infty d$ scaling when wake chemistry is important.

Case C. Wake Chemistry at High Velocity When $\chi_N > \chi_{NO}$

When the N flux into the wake becomes comparable to or exceeds the NO flux into the wake, two additional fast reactions must be included;

$$N + O_2 \xrightarrow{k_A} NO + O$$
$$N + NO \xrightarrow{k_A} N_2 + O \quad (13)$$

N atoms react with O_2 to make NO, or react with NO to make N_2. Reaction A increases while reaction B decreases the amount of NO. Reactions A and B are very fast and the N is used up in the early part of the turbulent wake. From the point of view of the NO_2 chemiluminescence, it is important to know the net NO production: this NO will flow into the far wake and produce the far wake NO_2 chemiluminescence. Reaction B is fast and temperature independent while reaction A is very temperature dependent, being fast above about 1000°K but becoming slow with decreasing temperatures. Thus, the net production depends sensitively upon the temperature of the volume element in which the N is mixed with the entrained O_2.

Since the reactions of N with the NO and O_2 depend intimately on the details of the turbulent mixing, experiments which determine the NO_2 chemiluminescence in the far wake should be a powerful method for evaluating near wake turbulent mixing models with chemistry.

The atomic O flux into the wake always exceeds that of atomic N or NO. Reactions A and B produce more O but not in sufficient amounts to appreciably change the total O. Since the atomic O is not affected appreciably, the NO_2 chemiluminescent radiation gives a measure of how much NO survives. There is no experimental data with which to compare the theoretical predictions, so we will not present, in this paper, a model which includes details of the chemiluminescence when N production is significant.

Scaling Relations: Summary

The simplest scaling relationship on body size is $p_\infty d = a$ const. With no wake chemistry (case A) the NO_2 chemiluminescent emission intensity exhibits approximate $p_\infty d$ scaling; χ_O and χ_{NO} have a small dependence on both $p_\infty d$ and body size. When wake chemistry is important and the NO_2 intensity decrease is due to atomic oxygen clean-up, the far wake intensity decay scales as $p_\infty{}^2 d$. Thus, depending upon the chemistry, the NO_2 chemiluminescent radiation decay can vary from $p_\infty d$ to $p_\infty{}^2 d$ scaling. Simple $p_\infty d$ scaling comparisons of ballistic range data with that for larger vehicles are in general not justified, except perhaps

Table 1 Reactions and rates used for far wake calculations (atomic N chemistry omitted)

No.	Reaction	Rate constant[a] A	B	C
1	$2O + O \rightarrow O_2 + O$	1.1 (29)	1.0	0
2	$O + 2O_2 \rightarrow O_3 + O_2$	4.1 (35)	0	900
3	$O + O_2 + N_2 \rightarrow O_3 + N_2$	3.5 (35)	0	900
4	$O + NO + M \rightarrow NO_2 + M$	4.0 (33)	0	970
5	$NO_2 + M \rightarrow NO + O + M$	2.6 (7)	0	−36300
6	$O + NO_2 \rightarrow NO + O_2$	3.0 (11)	0	−550
7	$NO + O_2 \rightarrow NO_2 + O$	3.3 (10)	0	−23600
8	$O + O_3 \rightarrow 2O_2$	1.4 (12)	0	−1500
9	$NO + O_3 \rightarrow NO_2 + O_2$	8.0 (13)	0	−1200
10	$NO_2 + O_2 \rightarrow NO + O_3$	1.1 (12)	0	−25100
11	$O + N_2O \rightarrow 2\,NO$	1.5 (10)	0	−14000
12	$2NO + O_2 \rightarrow 2NO_2$	2.0 (38)	0	0
13	$NO + O \rightarrow NO_2$	5.0 (13)	1.55	0
14	$NO_2 + O_3 \rightarrow NO_3 + O_2$	9.8 (12)	0	−3500
15	$NO_3 + N_2 \rightarrow NO + O_2 + N_2$	1.0 (13)	0	−2200
16	$NO + NO_3 \rightarrow 2NO_2$	1.0 (10)	0	−700
17	$2O + O_2 \rightarrow 2O_2$	4.1 (30)	−1.0	0
18	$2O + N_2 \rightarrow O_2 + N_2$	9.2 (31)	−1.0	0
19	$2O \rightarrow O_2$	7.1 (18)	0	−14450
20	$O + O_2 + O_3 \rightarrow 2O_3$	1.5 (34)	0	750
21	$O_3 + O_2 \rightarrow O + 2O_2$	3.4 (9)	0	−12000
22	$O_3 + N_2 \rightarrow O + O_2 + N_2$	3.2 (9)	0	−12000
23	$2O_3 \rightarrow O + O_2 + O_3$	7.7 (9)	0	−12000
24	$2O_2 \rightarrow O_3 + O$	1.1 (11)	0	−49600

[a] Form of rate constant is $k = AT^B \exp(C/T)$, where $A = x(10^{-n})$ is written as $x(n)$.

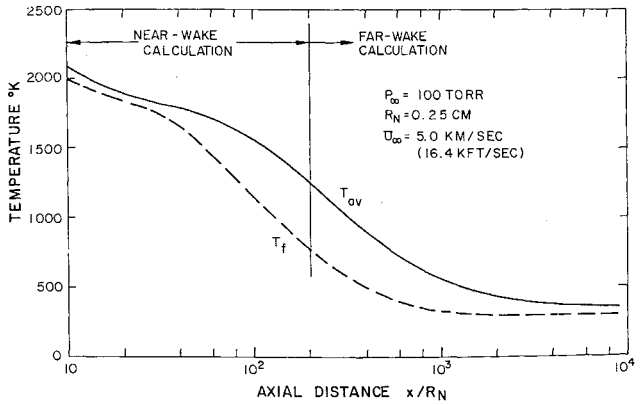

Fig. 8 Average wake and front temperatures for the same case as Fig. 7. The lag of T_{av} behind T_f beginning at $x/R_N \sim 40$ results from recombination of atomic oxygen.

within a narrow range around $p_\infty d \sim 0.01$. It is necessary to use complete flowfield calculations including nonequilibrium air chemistry to correlate the data from spheres of any size and velocity with the theory presented in this paper.

IV. Comparison of Calculations with Ballistic Range Data

The aerodynamic and chemical models discussed in the previous two sections were used to calculate NO_2 wake intensity for ballistic range experiments[1] performed at GM.†

Typical results from the wake calculation procedures are shown in Figs. 7 and 8; inviscid flowfield properties for this case were given previously. As indicated, the far-wake calculation is started at $x/R_N = 200$ with input values from a high-temperature near-wake calculation procedure.[6] Also plotted in Fig. 7 as the dashed line is the mole ratio of a dilute, passive mix; this quantity decreases solely by dilution. Thus, decay of NO concentration is seen to follow closely the pure dilution falloff, whereas at about $x/R_N \sim 1000$ the O mole ratio begins to decay faster than the pure dilution rate, signaling the onset of significant chemical effects. O_3 concentration builds up rapidly (Its initial value is zero), and attains a level comparable to NO and exceeding O around $x/R_N \sim 5000$. Note that the N concentration is far below that of NO or O, so that we are justified in ignoring the N chemistry. Hence, the amount of NO in the wake remains constant, and only atomic oxygen depletion effects the NO_2 wake emission in the range $x/R_N \lesssim 5000$.

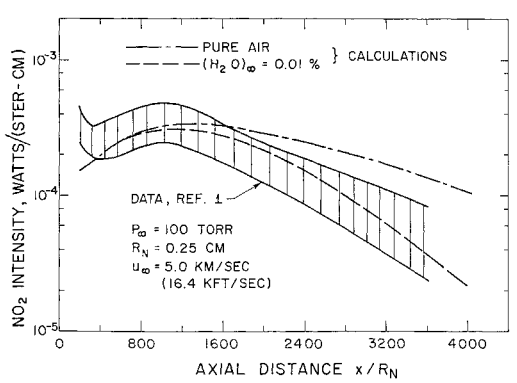

Fig. 9 Comparison of calculations with data of Ref. 1. Two theoretical results are given, one for pure air and the other for the indicated percentage by volume of water vapor in the freestream.

† General Motors Corporation, AC-Electronics, Defense Research Laboratories (AC-DRL).

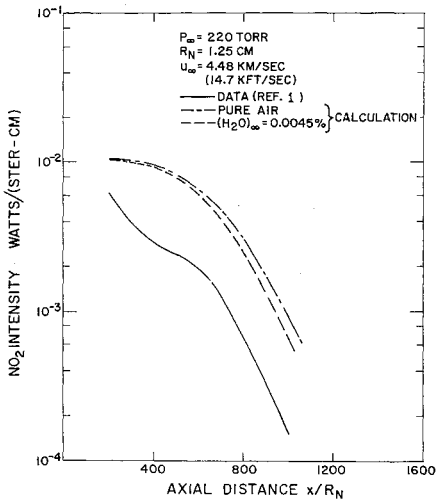

Fig. 10 Comparison of results from procedure described in text with data of Reis.[1] The two calculations were run for pure air and indicated percentage by volume of water vapor in the freestream.

From the results such as just shown the NO_2 wake radiation was computed for four ballistic range cases which are shown in Figs. 9–12. We have used a value for $\bar{\nu}$ corresponding to a wave length of 6200 Å, where the spectral distribution of NO_2 intensity peaks.[2]

Figures 9 and 10 include data published by Reis.[1] His intensities are given in units of w/ster-μ-cm for the radiometer band-pass from 0.6 to 0.7 μ. The factor which converts these values to w/ster-cm, i.e., to total intensities (integrated over wavelengths 0.4–1.4 μ) computed by the program, is 0.5; intensities in the 0.6–0.7 μ spectral region contribute 20% of the total radiation.[2]

In Fig. 9 for 100 torr, the pure-air calculation agrees well with the measurements near the intensity peak, but falls slightly above the data far downstream. Calculated intensity decay matches well that of the data.

Figure 10 presents the case at 220 torr but at slightly reduced speed. Calculated pure-air intensity levels differ from the data by a larger factor than at 100 torr, but far-wake intensity decay rates are in good agreement. In this case no intensity peak occurs because at these values of $p_\infty d$ (11 times $p_\infty d$ of Fig. 9) atomic O depletion is much more rapid than the temperature decrease at all axial stations.

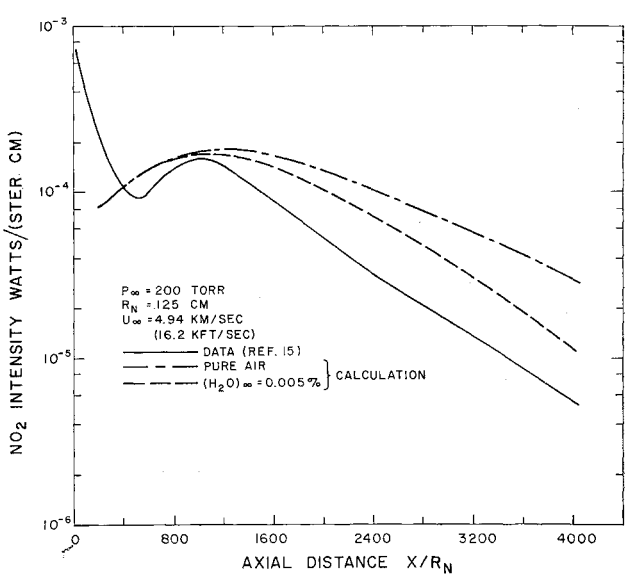

Fig. 11 Comparison of theoretical results to data of Ref. 15.

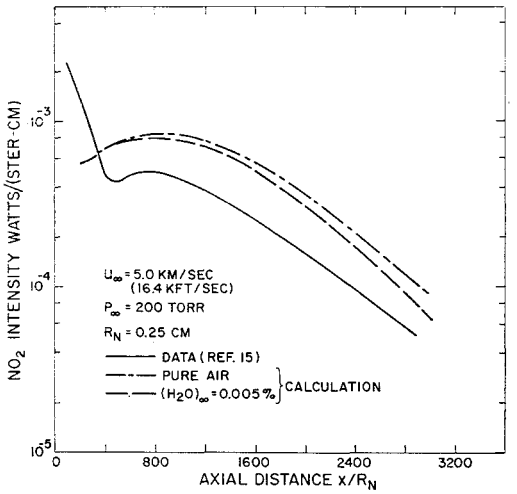

Fig. 12 Comparison of theoretical results to measurements given in Ref. 15.

In order to investigate the scaling, we include two unpublished runs of Reiss[15] at about the same velocity as for Fig. 9. Figure 11 shows the NO_2 intensity for a ballistic round with the same $p_\infty d$, at twice p_∞ of Fig. 9. According to the discussion of Sec. III, binary scaling should be fairly good up to the vicinity of the intensity peak. One sees that the intensities in Fig. 9 and 11 are within a factor of 2 out to $x/d \sim 800$. Both the data and calculation exhibit a decrease in the higher pressure case by about the same factor; this is partly a result of the slightly lower velocity.

Figure 12 presents data and prediction with $p_\infty d$ twice that of Figs. 9 and 11 at $U_\infty = 6.4$ kft/sec. With approximate binary scaling, peak intensities should be 2–4 times those of Fig. 9, which is borne out by the calculations. However, only a small increase is found in the data.

The importance of atomic O chemical depletion relative to dilution is illustrated for these cases in Fig. 13, where the atomic O mole ratio parameter is defined by Eq. (9). Curves 1 and 2 have the same $p_\infty d$, but 2 is at p_∞ twice that of 1. In these cases O chemistry is not very important, so one would expect approximate binary scaling at these values of $p_\infty d$ and lower. Curves 3 and 4 exhibit the $p_\infty{}^2 d$ scaling, which obtains for significant O chemistry. It is clearly seen that in case 4 the depletion of atomic O is so rapid that no peak occurs in the NO_2 intensity curve; the effect of atomic O chemistry on the amplitude of the intensity peak is already being felt in the case of curve 3 (see Figs. 9, 11, 12).

Effect of Water Vapor on NO_2 Intensity

During the course of these calculations, it was brought to our attention that a small amount of water vapor impurity had very likely been present in the AC-DRL experiments. Steinberg[16] of AC-DRL kindly furnished us with measurements of water vapor content obtained during a series of runs on the same range made several months prior to the shots reported by Reis.[1,15] The H_2O data are given in Ref. 8; it is indicated that about 0.01% water vapor by volume (100 ppm) could have been present at $p_\infty = 100$ torr. Assuming partial pressure of water vapor constant, the H_2O concentration at $p_\infty = 200$ torr would be 0.005%, and at $p_\infty = 220$ torr, 0.0045%. These are extrapolated values, since the measurements were made only up to $p_\infty = 100$ torr.

While these are relatively small amounts of water vapor impurity, the chemistry of atomic hydrogen is so fast that it can be an important factor in the atomic O cleanup.

Water vapor by itself is not important in the wake chemistry; however, the water vapor is converted to atomic hydrogen behind the strong portions of the bow shock. This hydrogen then flows into the near wake and is another constituent which must be considered in the wake chemistry.

In light of the uncertainty associated with the water vapor content during the NO_2 intensity runs, only an estimate was made of the initial hydrogen mole ratio in the wake. This was obtained by assuming that all water vapor intercepted by the body was dissociated into atomic hydrogen, justification being that atomic H is produced in hot regions where there is a high atomic O concentration. Calculations show that for the ballistic range cases herein considered, the atomic O mole ratio equals or exceeds the O_2 mole ratio along all stream lines which enter the bow shock at distances from the axis less than about 0.8 R_N; thus, the cross section for significant O production is very nearly the body area. Therefore, assuming that H chemistry freezes around the body until the H-bearing gas has completely entered the wake, the flux of H atoms produced behind the bow shock equals the flux through the wake

$$R_N{}^2 U_\infty 2[H_2O]_\infty = R_f{}^2 U_{av}[H]_{av}$$

Since the mole ratio

$$(X_H)_{av} \approx [H]_{av}/[M]_{av}$$

where

$$[M]_{av} T_{av} \approx [M]_\infty T_\infty$$

one has

$$(X_H)_{av} \approx 2\{[H_2O]/[M]\}_\infty (T_{av}/T_\infty) Y_f{}^{-2}$$

For the four ballistic cases cited at $X/R_N = 200$

$$2(T_{av}/T_\infty) Y_f{}^{-2} = 0.53$$

within a few %; the initial hydrogen mole ratio was thus $(X_H) \sim 2.5 - 5(10^{-5})$ at $x/R_N = 200$. At these concentrations, the thermodynamic effect of H on the wake flow was negligible.

Using these initial concentrations, the four cases corresponding to Figs. 9–12 were rerun to assess the effect of H chemistry.[8] The dashed curves in Figs. 9–12 show the NO_2 intensities including hydrogen chemistry. Departure from pure-air intensities begins at about the peak; far downstream the H chemistry has accelerated atomic O depletion

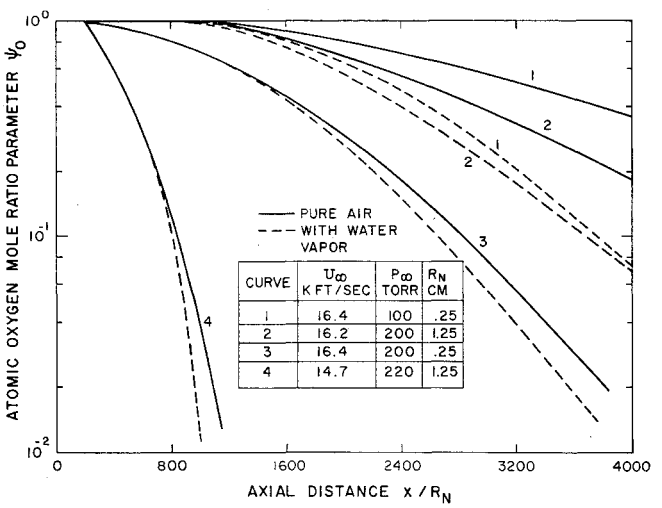

Fig. 13 The ratio of average atomic oxygen number densities with and without chemistry obtained from one-dimensional wake calculations. The effect of water vapor is indicated by the dashed curves (see Figs. 9–12 for ambient H_2O concentrations). The number density without chemistry decreases by pure dilution, so departure of ψ_o from unity gives effect of chemical O depletion.

sufficiently to produce a nonnegligible discrepancy in the NO_2 intensity decay of the 100-torr case (Fig. 9).

With the addition of hydrogen contamination, the agreement between measurements and predictions is improved. Unfortunately, the water vapor impurity levels were not monitored for these data, so we can only say that impurity concentrations suggested by previous range work give a more consistent over-all picture.

An important conclusion is that trace amounts of water vapor can appreciably affect observables which depend on chemistry of atomic oxygen. Note, however, that the NO_2 intensity peaks which occur at several hundred body diameters are not affected appreciably by the hydrogen impurity; thus, this region can be used to study the effects of bow shock chemistry for pure air conditions.

While the agreement between theory and experiment is considered good, one notes a tendency of the calculations to be higher than the data. We have attempted to evaluate any source of systematic error in both the data and computer programs. The uncertainty in range measurements reported by Reis[1] is represented by the hatched band in Fig. 9 and is his evaluation of the (random) data scatter. In addition, there could be a (systematic) bias in the data arising from instrument calibration, which Reis[15] estimates to be no greater than a factor of 2. Our calculations depend on chemical rate constants measured at bow-shock temperatures; these were determined in shock-tube experiments. Shock-tube measurements are accurate in general to about a factor of 2. We must also recognize that the basic inputs to the inviscid program, such as the pressure distribution and bow-shock shape, carry uncertainty into the flowfield properties which could be of a systematic nature. This is especially true of the shock shape, where the principal uncertainty lies in the shock slopes at axial positions downstream of the body. Stream lines in this region of the inviscid field undergo no chemistry, but nevertheless have sufficient thermal energy to appreciably affect the wake cooling rate, since they are ingested into the wake beyond the O, NO-entainment cutoff.

Taking all these aspects of the theory into account, one concludes that agreement between measurements and computations is satisfactory; a careful and more comprehensive set of measurements would be a severe test of the entire calculational scheme. As one develops more sophistication and confidence in ballistic range measurements, we will have an excellent tool for the study of aerodynamic as well as chemical phenomena.

References

[1] Reis, V. H., "Chemiluminescent Radiation from the Far Wake of Hypersonic Spheres," *AIAA Journal*, Vol. 5, No. 11, Nov. 1967, pp. 1928–1933.

[2] Fontijn, A., Meyer, C. B., and Schiff, H. I., "Absolute Quantum Yield Measurements of the NO-O Reaction and Its Use as a Standard for Chemiluminescent Reactions," *Journal of Chemical Physics*, Vol. 40, 1964, p. 64.

[3] Sutton, G. W. and Camac, M., "Wake-Temperature Turbulent Fluctuation Decay Rates Deduced from O_2 Radiation," *AIAA Journal*, Vol. 6, No. 12, Dec. 1968, pp. 2402–2409.

[4] Lin, S. C. and Teare, J. D., "A Streamtube Approximation for Calculation of Reaction Rates in the Inviscid Flow Field of Hypersonic Objects," AMP 77, 1961, Avco Everett Research Lab.; also *6th Symposium on Ballistic and Aerospace Technology*, Vol. 4, Academic Press, New York, 1962, p. 35.

[5] Sutton, E. A., "Chemistry of Electrons in Pure-Air Hypersonic Wakes," *AIAA Journal*, Vol. 6, No. 10, Oct. 1968, pp. 1873–1881.

[6] Lin, S. C. and Hayes, J. E., "A Quasi-One-Dimensional Treatment of Chemical Reactions in Turbulent Wakes of Hypersonic Objects" *AIAA Journal*, Vol. 2, No. 7, July 1964, pp. 1214–1222.

[7] Korkan, K. D., "Comments on 'Bow Shock Shape about a Spherical Nose'," *AIAA Journal*, Vol. 4, No. 2, Feb. 1966, pp. 381–382.

[8] Schapker, R. L. and Camac, M., "NO_2 Chemiluminescent Wake Radiation," Research Rept. 293, 1968, Avco Everett Research Lab.; also AIAA Paper 68-702, Los Angeles, Calif., 1968.

[9] Wilson, L. N., "Body-Shape Effects on Axisymmetric Wakes: Transition," *AIAA Journal*, Vol. 4, No. 10, Oct. 1966, pp. 1741–1747.

[10] Levensteins, Z. J. and Krumins, M. V., "Aerodynamic Characteristics of Hypersonic Wakes," *AIAA Journal*, Vol. 5, No. 9, Sept. 1967, pp. 1596–1602.

[11] Bailey, A. B., "Observations of Sphere Wakes Over a Wide Range of Velocities and Ambient Pressures," Rept. AEDC-TR-68-112, 1968, ARO Inc.

[12] Wilson, L. N., "Far Wake Behavior of Hypersonic Spheres," *AIAA Journal*, Vol. 5, No. 7, July 1967, pp. 1238–1244.

[13] Hartunian, R. A., Thompson, W. P., and Hewitt, E. W., "Glow-discharge Shock Tube for Studying Chemiluminescent, Surface-Catalytic, and Gas-Phase Reaction Rates; Temperature Dependence of the NO-O and CO-O Chemiluminescence," *Journal of Chemical Physics*, Vol. 44, 1966, pp. 1765–1769.

[14] Clyne, M. A. A. and Thrush, B. A., "Mechanism of Chemiluminescent Combination Reactions involving Oxygen Atoms," *Proceedings of the Royal Society*, Vol. A269, No. 404, 1962.

[15] Reis, V. H., private communication, Sept. 1967, Avco Everett Research Lab.

[16] Steinberg, M., private communication to V. Reis, Oct. 1967, General Motors Corp., AC-Electronics, Defense Research Labs.